

Head-Neck Dynamics in Frontal Impact: Obtaining Lower Neck Loads in PMHS

F. A. Pintar, M. B. Schlick, and N. Yoganandan

This paper has not been screened for accuracy nor refereed by any body of scientific peers and should not be referenced in the open literature.

ABSTRACT

The FMVSS-571.208 regulations contain injury criteria for the head, neck, chest, and femur. The neck injury criteria in particular include a check of axial neck forces and frontal plane bending moments. The upper neck force in tension and compression, and the upper neck flexion and extension moment are monitored in time and with respect to critical values. Recently, vehicle safety belt systems have undergone a variety of changes including belt pre-tensioning and belt load-limiting functions. It is not clear if these advanced belt systems have the potential to allow higher neck loads to occur. These belt systems also allow different head motion to occur depending on the body mass, occupant age, stature, crash severity, and other factors. Since a dummy's head motion is dictated largely by the biofidelity of the neck, established neck biofidelity criteria under different belt systems would allow for enhanced functioning of these advanced systems. The calculation of neck loads is a challenging task in PMHS. To provide meaning to the upper and lower neck loads recorded from dummies, a robust method of measurements and calculations is required. This paper outlines specific methodology and preliminary results from a series of frontal impact sled tests with both PMHS and dummies.

INTRODUCTION

The Federal Motor Vehicle Safety Standards (FMVSS) for protection in frontal impact include tests for belted mid-sized and small occupants up to 35 mph. Under the FMVSS-571.208, there are injury criteria for the head, neck, chest, and femur. The neck injury criteria in particular include a check of axial neck forces and frontal plane bending moments. The upper neck force in tension and compression, and the upper neck flexion and extension moment are monitored in time and with respect to critical values. The upper neck injury criteria is rarely exceeded in the Hybrid-III family of dummies under a belted FMVSS-208 test, except when the dummy's head and neck are in close proximity to a deploying airbag (Park et al., 1998). Some have argued that exceeding the neck injury criteria due to high bending moments may be more a function of the dummy design and not an actual risk of neck injury (Kang et al., 2005). In surveys of actual crashes, neck injuries in belted frontal impacts have been a relatively rare event (Augenstein et al., 1996; Huelke et al., 1981; Malliaris et al., 1982). This is perhaps why there has not been a high degree of active research in this area (Nightingale et al., 2002; Mertz and Patrick, 1971, Prasad and Daniel, 1984). Recently

however, vehicle safety belt systems have undergone a variety of changes including belt pre-tensioning and belt load-limiting functions (Yeh et al., 2005). It is not clear if these advanced belt systems have the potential to allow higher neck loads to occur. These belt systems also allow different head motion to occur depending on the body mass, occupant age, stature, crash severity, and other factors. Since a dummy's head motion is dictated largely by the biofidelity of the neck, established neck biofidelity criteria under different belt systems would allow for enhanced functioning of these advanced systems.

Despite the incorporation of the lower neck load cell into the measurement of dummy responses for many years, there have not been many uses for its output. Much of this has to do with the interpretation of the loads and understanding how the loads relate to injuries or biofidelity of the spine. Our general understanding of how load magnitudes relate to injury comes from Post Mortem Human Subject Specimens (PMHS) experiments. The calculation of neck loads at the occipital condyles of a PMHS is fraught with difficulty. The use of inverse dynamics equations to obtain these loads has been accomplished, but with little discussion of accuracy or the precision of measurements needed to obtain the desired outputs. Recently, our group has described the necessary technical requirements that improve the accuracy of obtaining upper neck loads in PMHS (Pintar et al., 2005). The goal of this paper is to present the methods and preliminary data to extend these techniques to obtain lower neck loads. The hypothesis that will be pursued is that lower neck loads may be a good indicator of the sensitivity of the head-neck complex to different belt restraint systems.

METHODS

A generic frontal impact test setup using a sled to apply accelerations was used. The generic frontal impact buck consisted of a rigid seat at specified angles (15 degree for seat pan and 25 degree for seat back) with an adjustable head restraint (front/back, up/down), and an adjustable knee bolster with 30 psi paper honeycomb used for padding. The adjustable nature of the buck will allow for different sizes of PMHS and dummies to load the restraint systems in the same orientation (Figure 1). The project goals include evaluation of Hybrid-III 50M, 95M, and 5F dummies as well as the THOR-NT dummy and compare results to PMHS. The knee bolster was adjusted for each occupant such that there was a 25 mm gap between the front of the knee/lower limb and the paper honeycomb. The head restraint was adjusted such that the center of the restraint was slightly in contact with the most rearward part of the head. A system of reflective targets were placed on various body regions and a VICON motion capture system was used to track motions in three dimensional space (Figure 2). A more detailed description of what was done with these target motions is given below. Tests were completed at three different speeds: low (3.3 m/s), medium (6.7 m/s), and high (15.7 m/s). As an initial evaluation of the test setup, a generic three-point belt system was designed using an adjustable D-ring and fixed anchor points behind and below the seat pan to mimic the locations in actual vehicles. The belt was given one of three types of pretension: low-tension by hanging a 1 kg weight on the belt below the D-ring; force-pretension by applying 200 N of load on the belt; displacement-pretension by applying 10 cm of displacement on the belt. The latter two configurations were done after the 1 kg load was hung from the belt below the D-ring. A detailed description of the data collection procedures and analysis is provided.



Figure 1: Generic rigid seat sled buck for frontal impact testing.



Figure 2: The THOR-NT dummy shown in the test setup with reflective markers.

Data Collection and Analysis

Pre-event Data Collection. Instrumentation axes were aligned to follow the SAE-J211 axes system. Records of all axes and polarities and locations were photographed whenever possible including sensor S/N's. Once the data acquisition system (DAQ) was plugged-in and set-up, a final, independent audit/record of channels and S/N's was done. The instrumentation sample frequency was 12,500 Hz. In the future, a 20,000 Hz frequency will be used as this is a multiple of 1,000 Hz and the data can later be sub-sampled to point-by-point coincide with motion capture data (VICON) which have a maximum sample rate of 1,000 Hz. The channels collected are given as:

- Primary Sled Acceleration
- Redundant Sled Acceleration
- Tzero Floor Switch
- Sled Velocity Gear Tooth Sensor (Yellow)
- UniDir. Sled Velocity Gear Tooth Sensor (Green)
- Sled Velocity (Tach)
- Plunger t0 switch
- HEAD CG ACC X
- HEAD CG ACC Y
- HEAD CG ACC Z
- HEAD NAP LEFT X
- HEAD NAP LEFT Y
- HEAD NAP LEFT Z
- HEAD NAP FRONT X
- HEAD NAP FRONT Y
- HEAD NAP FRONT Z
- HEAD NAP TOP X
- HEAD NAP TOP Y
- HEAD NAP TOP Z
- T4 ACC X
- T4 ACC Y
- T4 ACC Z
- PELVIS ACC X
- PRIMARY PELVIS ACC Y
- REDUNDANT PELVIS ACC Y
- PELVIS ACC Z
- UPPER NECK LOADCELL FX
- UPPER NECK LOADCELL FY
- UPPER NECK LOADCELL FZ
- UPPER NECK LOADCELL MX
- UPPER NECK LOADCELL MY
- UPPER NECK LOADCELL MZ
- LOWER NECK LOADCELL FX
- LOWER NECK LOADCELL FY

LOWER NECK LOADCELL FZ
LOWER NECK LOADCELL MX
LOWER NECK LOADCELL MY
LOWER NECK LOADCELL MZ
CHEST POT
LOWER RIGHT SEAT BOTTOM LOAD X
LOWER RIGHT SEAT BOTTOM LOAD Y
LOWER RIGHT SEAT BOTTOM LOAD Z
UPPER RIGHT SEAT BOTTOM LOAD X
UPPER RIGHT SEAT BOTTOM LOAD Y
UPPER RIGHT SEAT BOTTOM LOAD Z
LOWER LEFT SEAT BOTTOM LOAD X
LOWER LEFT SEAT BOTTOM LOAD Y
LOWER LEFT SEAT BOTTOM LOAD Z
UPPER LEFT SEAT BOTTOM LOAD X
UPPER LEFT SEAT BOTTOM LOAD Y
UPPER LEFT SEAT BOTTOM LOAD Z
Seatbelt Shoulder Load Cell
Seatbelt Lap Load Cell
T1 ACC X
T1 ACC Y
T1 ACC Z
T1 ANGULAR VELOCITY X
T1 ANGULAR VELOCITY Y
T1 ANGULAR VELOCITY Z

Motion Capture Using VICON System. To each rigid body of interest (including but not limited to: Head, T1, Sled) no less than 4 or 5 non-collinear, reflective markers were secured to aspects that were expected to remain visible to many of the 20 cameras throughout the event and were not expected to contact other bodies. The placement and orientation of each marker set followed SAE-J211 axes as closely as possible. The VICON motion capture sample rate was 1,000 Hz.

Digitized Static Points of Interest Using FARO arm. On each rigid body, marker sets and instrumentation packages and “anatomy” defining points and three reference points were digitized with respect to a single reference system as follows:

All reflective spherical markers.

12 instrumentation axes defining points if necessary (i.e. any transducers mounted to surfaces of unknown axes like those mounted to the surface of a PMHS head in contrast to those mounted, for example, at the dummy head CG), 4 points each for 3 mutually orthogonal axes; where three non-collinear points define a plane (typically the plane in which one sensor is affixed) and the fourth defines the tip of the vector, orthogonal to that plane, defining the positive sensitive axis of the transducer in direction and location. The axis label (typically “X,” “Y,” or “Z”) and polarity were meticulously matched to those in the DAQ.

“Anatomy” defining points: For example for the PMHS head: auditory meatus (“LAud,” “RAud”) and infra-orbital notches (“LOrb,” “ROrb”) such that the Frankfurt Plane can be quantitatively identified; for the seat/sled: a front point and back point on a left-right mid-line, and a left point and a right point on a front-back mid-line, and an origin point. Three permanently marked, non-collinear, control points used to define the current and future relationship between digitizer and rigid body.

Other points: Points useful in defining aspects of the rigid body not explicit in the markers. (For example, if the seat and the sled were treated as one rigid body but there were only markers on the sled, the four corners of the seat bottom were digitized and later brought into the motion capture data and displayed frame-by-frame in coordination with the sled marker motions.)

PMHS Clinical Assessment: Boney landmarks and physiologic motions were examined, palpated, and x-rayed prior to the experiment and as soon as possible post test.

Post-Event Data Collection: Following the event each rigid body was re-oriented to the digitizer using the three control points and then all the pre-event points were re-digitized in case markers were inadvertently moved with respect to the rigid body during the event. Also, rigid bodies were later isolated and points not available non-destructively before the event were digitized with respect to the original digitizer-body orientation. For the Head: exterior CG reference points as identified below (2 points “HdCGL,” “HdCGR”); and the most inferior aspect of each occipital condyle (2 points “OCL,” “OCR”). For T1: the left most lateral point and right most lateral point of the approximated mid-coronal plane of the vertebral body at both the superior and inferior end-plates (4 points “T1VBSupL,” “T1VBSupR,” “T1VBInfL,” “T1VBInfR”); the most anterior point and most posterior point of the approximated mid-sagittal plane at both the superior and inferior end-plates of the vertebral body (4 points “T1VBSupF,” “T1VBSupB,” “T1VBInfF,” “T1VBInfB”); the most posterior-inferior point of the spinous process (1 point “T1SP”); and the left most lateral point of the left transverse process and right most lateral point of the right transverse process (2 points).

Isolated Head Mass, CG, and MOIs Measured: The PMHS head was isolated by dissecting between the occipital condyles and the C1 vertebra. The dissection line extended outward along the inferior margin of the mandible, the inferior aspect of the mastoid process, and the inferior margin of the occipital bone of the skull. Center of gravity and inertial properties of the head were measured according to methods outlined by the American National Standards Institute. Annex D of the standard specifies a methodology for chain saws using mechanics equations. The same method was adapted to PMHS head with the following modifications. Measurements were made on the frozen isolated head. For the center of gravity, the same method described in the Standard was used except eyelets were screwed into the midsagittal plane to facilitate cable suspension. To measure the moment of inertia, the same method described in the standard using a triangular aluminum plate suspended by three wires was incorporated. The PMHS head was balanced on the plate such that anatomical axes described above were coincident with the rotational axis of the plate. The process was repeated for each orthogonal anatomical axis.

Calculations: It is critical to maintain a one axes system and rigidly adhere to vector algebra principles from the very beginning of all data collection / measurements through final calculations.

Angular Velocities and Angular Accelerations: If a Pyramid Nine Accelerometer Package (PNAP) was used, the angular accelerations were calculated using the following equations:

$$\alpha_x = \frac{(A_{z1} - A_{z0})}{2R_{y1}} - \frac{(A_{y3} - A_{y0})}{2R_{z3}}$$

$$\alpha_y = \frac{(A_{x3} - A_{x0})}{2R_{z3}} - \frac{(A_{z2} - A_{z0})}{2R_{x2}}$$

$$\alpha_z = \frac{(A_{y2} - A_{y0})}{2R_{x2}} - \frac{(A_{x1} - A_{x0})}{2R_{y1}}$$

Where α is the angular acceleration, A is the linear acceleration, and R is the distance between the linear accelerometers. The angular velocities were calculated by integrating the angular accelerations. In the case where angular velocity sensors are used, the angular accelerations were calculated by differentiating the angular velocities.

Head Axes: The Frankfurt Plane defined the PMHS anatomical axes with the CG as the origin and all digitized head points were projected onto this axes system. The axes were derived via:

Calculating the midpoint (“MidAud”) between “LAud” and “RAud,” and the midpoint (“MidOrb”) between “LOrb” and “ROrb.”

Defining the +Y axis as from “LOrb” to “ROrb.”

Defining a temporary +X vector as from “MidAud” to the “MidOrb.”

Calculating the +Z axis as [+X temp-vector] X [+Y axis].

Calculating the +X axis as [+Z axis] X [+Y axis].

T1 Axes: The T1 axes were determined using the vertebral body with the origin at the posterior mid-sagittal point of the superior end-plate and all digitized T1 points were projected onto this axes system. The X and Y axes were based off both the superior and the inferior end plates (Figure 3). The axes were derived via:

- Calculating the mid-point (“T1VBMidB”) between “T1VBSupB” and “T1VBInfB.”
- Calculating the mid-point (“T1VBMidF”) between “T1VBSupF” and “T1VBInfF.”
- Defining +X direction as from the “T1VBMidB” to ”T1VBMidF.”
- Calculating the mid-point (“T1VBMidL”) between “T1VBSupL” and “T1VBInfL.”
- Calculating the mid-point (“T1VBMidR”) between “T1VBSupR” and “T1VBInfR.”
- Defining a temporary +Y vector as from “T1VBMidL” to ”T1VBMidR.”
- Calculating the +Z direction as [+X vector] cross [temporary +Y vector].
- Calculating the +Y direction as [+Z vector] cross [+X vector].
- Make “T1VBSupB” origin.

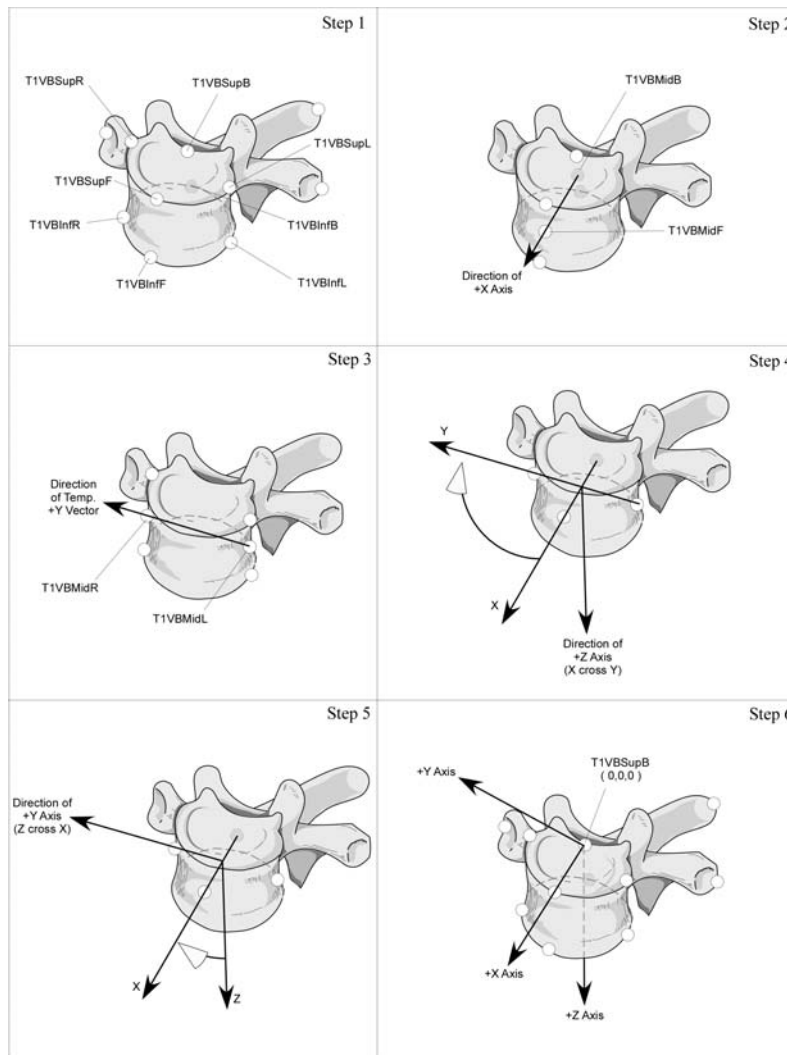


Figure 3: Derivation of T1 anatomical axes.

Individual Instrumentation Axes: Three mutually orthogonal axes were determined using the projected 12 digitized points on each sensor / sensor group as listed above via:

- Defining a plane using three points on the “Y” surface.

Defining the direction of the Y axis as the vector normal to this plane in the direction of the fourth “Y” (“positive sensitivity”) point.

Defining another plane using the three points on the “Z” surface.

To ensure orthogonality:

Defining the direction a temporary Z vector as the vector normal to this Z plane in the direction of the fourth “Z” (“positive sensitivity”) point.

Calculating the X axis as [Y axis] cross [temp Z vector].

Calculating the Z Axis as [X Axis] cross [Y Axis].

Computing, as a check, the difference between the X Axis and the vector normal to the X plane as well as the difference between the Z Axis and the vector normal to the Z plane. A typical difference of less than $\sim 0.5^\circ$ indicated the accuracy of the measurements and/or the accuracy of the orthogonality of the sensor body / sensor mounts.

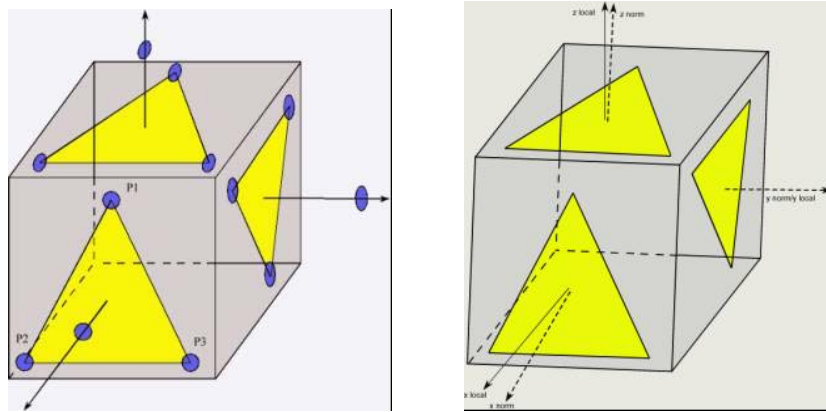


Figure 4: 12 point method for determining instrumentation package axes (left) and difference between normal vector and cross-product axes (right).

Equation for a Plane: $Ax + By + Cz + D = 0$

$$A = P1Y * (P2Z - P3Z) + P2Y * (P3Z - P1Z) + P3Y * (P1Z - P2Z)$$

$$B = P1Z * (P2X - P3X) + P2Z * (P3X - P1X) + P3Z * (P1X - P2X)$$

$$C = P1X * (P2Y - P3Y) + P2X * (P3Y - P1Y) + P3X * (P1Y - P2Y)$$

$$D = -1.0 * (P1X * (P2Y * P3Z - P3Y * P2Z) + P2X * (P3Y * P1Z - P1Y * P3Z) + P3X * (P1Y * P2Z - P2Y * P1Z))$$

Calculate angle(s) between Instrumentation Axes and Rigid Body Axes: Once the axes of the rigid body were determined and all the digitized points (including anatomy points, markers, and instrumentation points) were projected onto these anatomic axes and then the subsequent instrumentation axes were determined, the transformation matrix from the anatomic axes to the instrumentation axes was calculated. This transformation matrix was then abbreviated as three ordered XYZ Euler Angles each based off the anatomic axes.

Project Instrumentation Signals onto Rigid Body Axes: For each instrumentation package, such as three linear accelerometers, the entire time histories of the measured signals were projected onto the anatomic axes of the rigid body to which they were affixed, using the XYZ Euler angles calculated above. Again, each (x,y,z) projection was computed based off the anatomic axes.

Head CG Accelerations Computed: The linear accelerations at the head CG were computed using the projected signals of both the linear accelerometers and the angular accelerations from the PNAP and/or the angular velocities from the angular rate sensors (Yoganandan et al., 2006) using the following equations:

$$Acg_x = As_x + r_x(\omega_y^2 + \omega_z^2) - r_y(\omega_y\omega_x - \alpha_z) - r_z(\alpha_y + \omega_z\omega_x)$$

$$Acg_y = As_y - r_x(\alpha_z + \omega_x\omega_y) + r_y(\omega_x^2 + \omega_z^2) - r_z(\omega_z\omega_y - \alpha_x)$$

$$Acg_z = As_z - r_x(\omega_x\omega_z - \alpha_y) - r_y(\omega_y\omega_z + \alpha_x) + r_z(\omega_x^2 + \omega_y^2)$$

Where Acg is the linear acceleration calculated at the CG and As is the linear accelerometer signal and r is the distance from the CG to the linear accelerometer; ω is the angular velocity of the head and α is the angular acceleration of the head.

Forces at the Occipital Condyles (OC): The forces acting on the head, by the neck, were calculated by multiplying the mass of the head by the CG linear accelerations. Forces (and moments described below) were calculated as if acting at the traditional, virtual point of load, that is, the mid-point between the left and right occipital condyles. It should be noted that the force calculations are only valid when there are no other head contacts such as chin-to-chest or head-to-head rest (Figure 5).

Moments at the OC: The moments acting on the head by the neck were computed by calculating the total moment at the CG about each axes using the mass moment of inertia (as calculated above) with the on-axis angular acceleration, and the off-axis moments of inertia with the off-axis angular velocities and then combining the cross products produced by the forces at the OC using the following equations:

$$M_{ocx} = (I_{xa} * \alpha_x) + [(I_{za} - I_{ya}) * \omega_y * \omega_z] - (r_y \times F_z + r_z \times F_y)$$

$$M_{ocy} = (I_{ya} * \alpha_y) + [(I_{xa} - I_{za}) * \omega_z * \omega_x] - (r_z \times F_x + r_x \times F_z)$$

$$M_{ocz} = (I_{za} * \alpha_z) + [(I_{ya} - I_{xa}) * \omega_x * \omega_y] - (r_y \times F_z + r_z \times F_y)$$

Where M is the moment calculated at the OC, I is the mass moment of Inertia, α is the angular acceleration, ω is the angular velocity, r is the distance from the OC to the CG, and F is the force at the OC.

Linear and Angular displacements: The displacement of the head with respect to T1 was calculated from data collected through the VICON system by:

Defining a temporary, arbitrary axes system based on the markers and projecting all FARO digitized data (of anatomy points, etc.) onto these axes and exporting these projected data into an appropriately formatted VICON model parameter (.mp) file. Composing a VICON model file (.mod) wherein the identical, temporary axes system was defined. Importing the .mp data in that model. Re-defining an anatomically based axes system in the model, the identical system used with the FARO digitized and calculated data above. Computing all linear and angular displacements based on the anatomic axes system in the model. Computationally “over-sampling” these 1000 Hz sampled based data to match the instrumentation sample rate. (It should be noted that although SAE J211 CFC 1000 data were collected by the head instrumentation, calculations using these displacements such as the T1 forces and moments below, should not be considered to have captured the entire CFC 1000 frequency spectrum.) Carefully demonstrating that the angular displacements produced by the VICON model expressed as Euler Angles were the same Euler Angles used in all projections above in order, “parent” vs. “child,” and “fixed” rotations vs. “floating” rotations.

Forces and Moments at T1: A mass-less, single link neck was presumed for calculations and the forces at the head OC were projected onto the T1 axes using the VICON angular displacement data at every point in time (Figure 5). The moments at T1 were also based on a mass-less, single link neck and computed by:

Projecting the head OC moments onto the T1 axes using the VICON angular displacement data at every point in time. Combining the cross product moments produced by the forces at the OC.

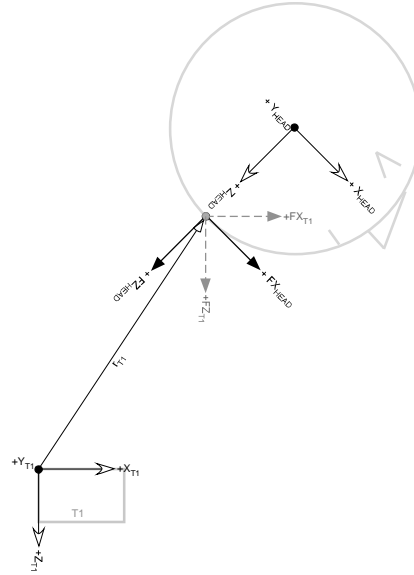


Figure 5: Schematic of coordinate systems used to obtain OC and T1 loads.

Forces and Moments at T1 from HIII Dummy Load Cell: The above computations were validated using a HIII 50% dummy by computing the OC and T1 forces and moments and comparing to the dummy's upper and lower neck load cells respectively. However before the load cells could be used for comparison, they also had to be "translated" to the anatomic points of interest. In the case of the upper neck, the signal was "translated" from the load cell's center of sensitivity to the center of the neck "Pivot Pin." In the case of the lower neck, particularly the adjustable lower neck load cell such as the R.A. Denton Model 2992, the signals must be "translated" and "rotated" according to the following:

$$r_{xT1} = (r_{xLC} \cdot \cos\theta_y) + (r_{zLC} \cdot \sin\theta_y)$$

$$r_{yT1} = r_{yLC}$$

$$r_{zT1} = (r_{zLC} \cdot \cos\theta_y) - (r_{xLC} \cdot \sin\theta_y)$$

$$F_{xT1} = (F_{xLC} \cdot \cos\theta_y) + (F_{zLC} \cdot \sin\theta_y)$$

$$F_{yT1} = F_{yLC}$$

$$F_{zT1} = (F_{zLC} \cdot \cos\theta_y) - (F_{xLC} \cdot \sin\theta_y)$$

$$M_{xT1} = [(M_{xLC} \cdot \cos\theta_y) + (M_{zLC} \cdot \sin\theta_y)] + -\{[(r_{zLC} \cdot \cos\theta_y) - (r_{xLC} \cdot \sin\theta_y)] \cdot F_{yLC}\}$$

$$M_{yT1} = M_{yLC} + (r_{zLC} \cdot F_{xLC}) - (r_{xLC} \cdot F_{zLC})$$

$$M_{zT1} = [(M_{zLC} \cdot \cos\theta_y) - (M_{xLC} \cdot \sin\theta_y)] + \{[(r_{xLC} \cdot \cos\theta_y) + (r_{zLC} \cdot \sin\theta_y)] \cdot F_{yLC}\}$$

Where throughout the first subscript letter defines the axis and the next two subscript characters define the axes system; r is the distance between the load cell's center of sensitivity and the center of the base of the neck 0.125" above the bracket (at the top surface of the "Bib" flap) – note axes system each time; θ is the angle between the base of the load cell and the base of the neck; F is the force; and M is the moment.

RESULTS

As a first step in verification of the methods, the Hybrid-III-50M dummy was used in a medium speed frontal impact test with a standard three point belt with low pretension. The dummy was instrumented with a nine-accelerometer package (NAP) and upper and lower neck load cell transducers. The upper neck loads were calculated using the NAP data and checked with what was recorded directly by the load cell (Figure 6). It can be seen that the calculated loads match reasonably well in shape and magnitude. The spike in the calculated dynamics data at approximately 200 msec is due to chin-to-chest contact wherein assumptions made for inverse dynamics calculations are no longer valid.

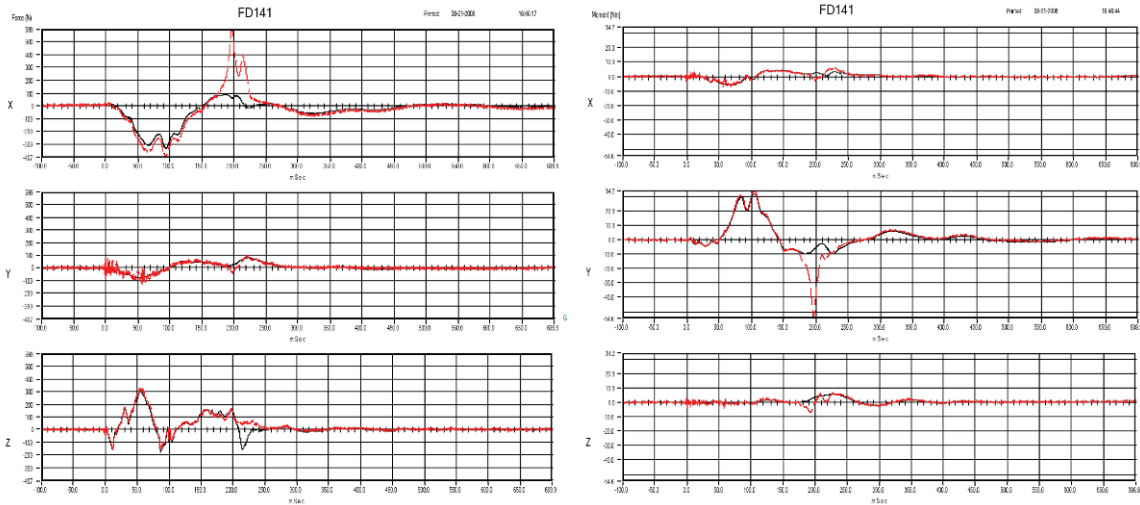


Figure 6: Comparison between calculated (red curves) upper neck loads and measured (black curves) for a dummy test. Forces are on the left graph and moments are on the right graph.

The lower neck loads were calculated using the NAP data and also compared to what was recorded directly by the load cell (Figure 7). Although not as good as the upper neck loads, it can be seen that the calculated loads match reasonably well.

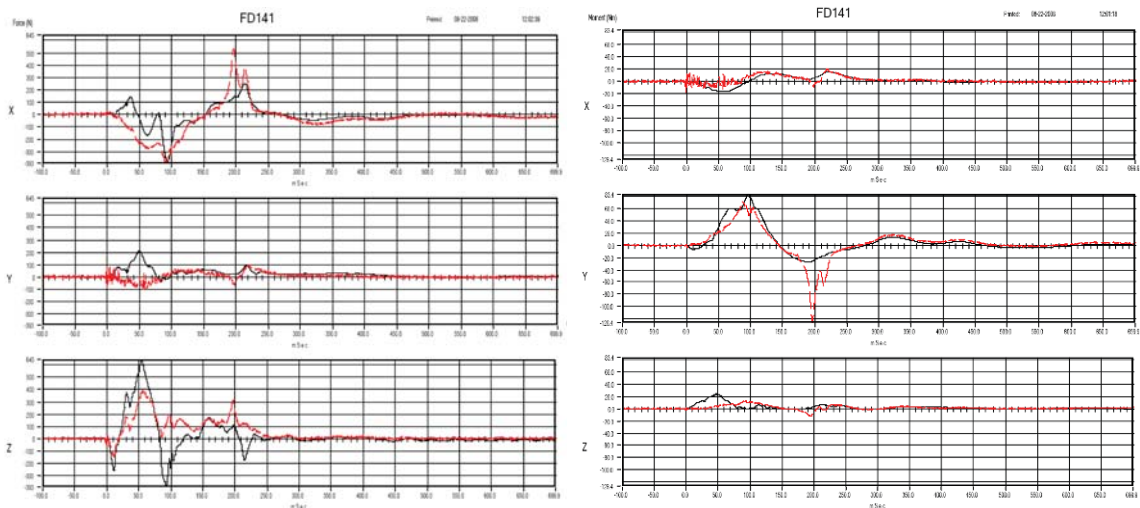


Figure 7: Comparison between calculated (red curves) lower neck loads and measured (black curves) for a dummy test. Forces are on the left graph and moments are on the right graph.

A PMHS was run using a standard 3-point belt restraint at low, medium, and high speeds and data was collected to obtain upper and lower neck loads. Since the head accelerometer instrumentation included a PNAP and a redundant tri-axial block, both of these accelerometer packages were used to originate calculations of upper and lower neck loads. In Figures 8 and 9, the black and red curves indicate the two sources used in the calculations.

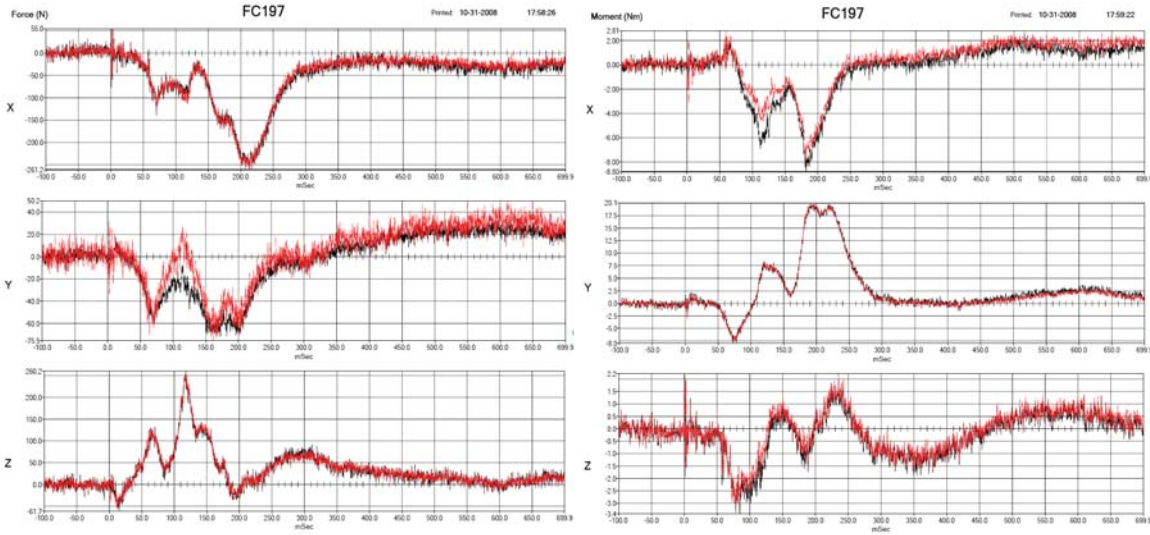


Figure 8: Upper neck forces (left) and moments (right) calculated for PMHS test FC197.

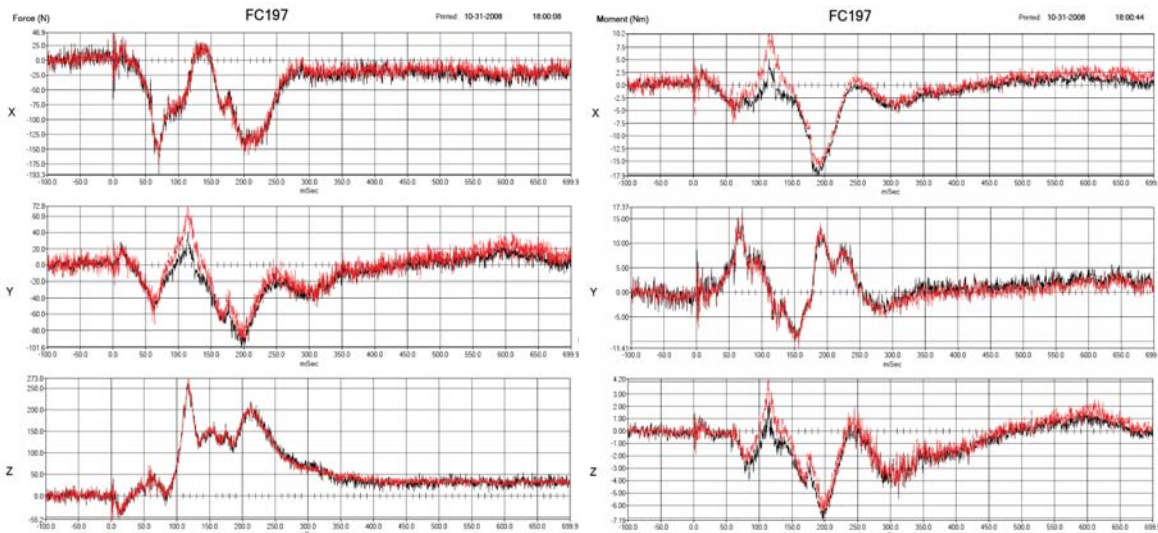


Figure 9: Lower neck forces (left) and moments (right) calculated for PMHS test FC197.

CONCLUSIONS

The calculation of neck loads is a challenging task in PMHS. To provide meaning to the upper and lower neck loads recorded from dummies, a robust method of measurements and calculations is required. This paper outlines specific methodology and preliminary results from a series of frontal impact sled tests with both PMHS and dummies.

ACKNOWLEDGEMENTS

This research was supported in part by the US DOT NHTSA under a cooperative agreement and by the Department of Veterans Affairs Medical Research. We are grateful to Ola Bostrum of Autoliv Sweden for supplying the belt webbing.

REFERENCES

- AUGENSTEIN, J., DIGGES, K PERDECK, E., LOMBARDO, L., and MALLIARIS, A. (1996). Injuries sustained by air bag protected drivers. SAE World Congress, Paper#960660. Society of Automotive Engineers, Warrendale, PA.
- CHENG, R., YANG, K., LEVINE, R., KING, A., and MORGAN, R. (1982). Injuries to the cervical spine caused by a distributed frontal load to the chest. 26th Stapp Car Crash Conf, Ann Arbor, MI.
- HUELKE, D., O'DAY, J., and MENDELSON, R. (1981). Cervical injuries suffered in automobile crashes. J Neurosurg, 54, 316-322.
- KANG, J., NUSHOLTZ, G., and AGARAM, V. (2005). Hybrid III Dummy Neck Issues. SAE World Congress, Paper#2005-01-1704. Society of Automotive Engineers, Warrendale, PA
- MERTZ, H. J. and PATRICK, L. M. (1971). Strength and response of the human neck. 15th Stapp Car Crash Conf (SAE Paper No. 710855).
- MALLIARIS, A. C., HITCHCOCK, R., and HEDLUND, J. (1982). A search for priorities in crash protection. SAE International paper #820242. Society of Automotive Engineers, Warrendale, PA.
- NIGHTINGALE, R., WINKELSTEIN, B., KNAUB, K., RICHARDSON, W., LUCK, J., and MYERS, B. (2002). "Comparative strengths and structural properties of the upper and lower cervical spine flexion and extension." J Biomech, 35, 725-732.
- PARK, B. T., MORGAN, R. M., HACKNEY, J. R., PARTYKA, S., KLEINBERGER, M., SUN, E., SMITH, H. E., and LOWRIE, J. C. (1998). Upper Neck response of the belt and air bag restrained 50th percentile hybrid III dummy in the USA's new car assessment program. 42nd Stapp Car Crash Conference, SAE paper #983164.
- PINTAR, F. A., YOGANANDAN, N., and BAISDEN, J. B. (2005). Characterizing Occipital Condyle Loads Under High-Speed Head Rotation. Stapp Car Crash Journal. Vol 49, pp 33-47.
- PRASAD, P. and DANIEL, R. P. (1984). A biomechanical analysis of head, neck, and torso injuries to child surrogates due to sudden torso acceleration. 28th Stapp Car Crash Conf, SAE paper #841656.
- YEH, I., KACHNOWSKI, B., and SUBBIAN, T. (2005). An expert system for vehicle restraint system design. SAE World Congress, Paper#2005-01-1304. Society of Automotive Engineers, Warrendale, PA
- YOGANANDAN, N., ZHANG, J., PINTAR, F., and LIU, Y. (2006). Lightweight low-profile nine-accelerometer package to obtain head angular accelerations. J Biomech. 39:1347-1354.

DISCUSSION

PAPER: **Head-Neck Dynamics in Frontal Impact: Obtaining Lower Neck Loads in PMHS**

PRESENTER: *Frank Pintar, Medical College of Wisconsin*

QUESTION: *Richard Kent, UVA*

I have one question, but it has three parts. First of all, thanks for embarking upon this. This is sort of a holy grail of cadaver testing, so this will be great. A couple of questions: One thing I noticed is that you actually had moment in the neck going up when you had pre-tensioning in the restraint system. So if you do that in a more vehicle-like, you typically don't see that. You see neck loads go down with pre-tensioning and load limiting and that sort of thing. It has to do with the pelvic motion. So I wonder if you might—just as a suggestion—take a look at the way you're constraining the pelvis. The one-inch offset between the knees and the knee bolster may be artificially holding the pelvis back in a way that wouldn't happen in, for example, a rear-seat environment, which I've been testing lately. And so, the pre-tensioner plays a big role in the pelvic motion, which you may be sort of filtering out with the way that you're controlling the lower body motions, especially with a flat plate instead of an automotive seat underneath the pelvis. So one suggestion to consider is that what might be an interesting thing to consider in your test matrix is what you let the lower body do.

ANSWER: Are you saying I should keep it farther away from the knee bolster?

Q: I'm saying you might be taking away one of the big effects of a pre-tensioner by controlling that pelvis motion with such a small gap between the knee and the knee bolster. So that may actually vary with the pre-tensioning, if you let it. That's the one idea.

A: That's a nice comment. Let's look into that. We can certainly—We want to make sure that this test set-up is as realistic as possible but still be generic.

Q: So the pre-tensioner is typically associated with a force limiter. And so when you have those two things together, the pre-tensioner keeps the pelvis back; the force limiter lets the torso pitch; and, the neck loads go way down. And so, you may have an interaction there that you missed if you constrain the pelvis too closely. So that's just a thought.

A: Okay.

Q: One other thing: I noticed you don't have any markers on the belt. We've been putting markers along the belt, which really helps you understand the kinematics you're getting, where those loads are going into the chest. So another thought. And then finally—

A: We were counting on you for that! [laughter]

Q: I can show up and glue them on! This is actually the first question. What's the point? How do you define the point where you calculate these forces in moment in the lower neck? Is it the middle of the vertebral body?

A: Yes. That's a question that I think we have to answer because even the dummies don't have the same point. The graphs I showed you are not at the same point. That's why I said they're preliminary. So, we do need to define—Like we did for the upper neck, we decided occipital condyles. That's the point that we're going to all call our upper-neck load cell. So we need to do that for the lower-neck load cell. I agree. We have to take whatever the dummies give us and say, "Okay. Let's define a point, whatever it is: top surface of T-1." Right now, we're using the middle of the vertebral body and the top surface of T-1, but it's arbitrary. We have to define that point and then say, "That's our standard where we take everything to."

Q: But how do you get that with a Faro Arm?

A: You have to digitize it afterwards. So in the dissection procedure, you have to have the mount on there with the targets and dissected to the T-1.

Q: Okay. So then another suggestion: The way we've been doing that is to take a CT after you get all the markers mounted on, and then you can do things like the middle of the volume of the disk or whatever you want. So you get a little more flexibility.

A: That's another way.